Bispecific Targeting of PD-1 and PD-L1 Enhances T-cell Activation and Antitumor Immunity

Helen Kotanides, Yiwen Li, Maria Malabunga, Carmine Carpenito, Scott W. Eastman, Yang Shen, George Wang, Ivan Inigo, David Surguladze, Anthony L. Pennello, Krishnadatt Persaud, Sagit Hindi, Michael Topper, Xinlei Chen, Yiwei Zhang, Danielle K. Bulaon, Tim Bailey, Yanbin Lao, Bing Han, Stacy Torgerson, Darin Chin, Andreas Sonyi, Jaafar N. Haidar, Ruslan D. Novosiadly, Christopher M. Moxham, Gregory D. Plowman, Dale L. Ludwig, and Michael Kalos

ABSTRACT

The programmed cell death protein 1 receptor (PD-1) and programmed death ligand 1 (PD-L1) coinhibitory pathway suppresses T-cell–mediated immunity. We hypothesized that cotargeting of PD-1 and PD-L1 with a bispecific antibody molecule could provide an alternative therapeutic approach, with enhanced antitumor activity, compared with monospecific PD-1 and PD-L1 antibodies. Here, we describe LY3434172, a bispecific IgG1 mAb with ablated Fc immune effector function that targets both human PD-1 and PD-L1. LY3434172 fully inhibited the major inhibitory receptor–ligand interactions in the PD-1 pathway. LY3434172 enhanced functional activation of T cells *in vitro* compared with the parent anti–PD-1 and anti–PD-L1 antibody combination or respective monotherapies. In mouse tumor models reconstituted with human immune cells, LY3434172 therapy induced dramatic and potent antitumor activity compared with each parent antibody or their combination. Collectively, these results demonstrated the enhanced immunomodulatory (immune blockade) properties of LY3434172, which improved antitumor immune response in preclinical studies, thus supporting its evaluation as a novel bispecific cancer immunotherapy.

Introduction

Targeting of the programed cell death protein 1 receptor (PD-1)/programmed death ligand 1 (PD-L1) coinhibitory pathway (PD-1 pathway) with mAbs has transformed cancer treatment. There are several regulatory approved agents that target both PD-1 (nivolumab, pembrolizumab, cemiplimab, sintilimab, and tislelizumab) and PD-L1 (atezolizumab, avelumab, and durvalumab) across a broad range of malignancies (1, 2). Although PD-1 pathway–based cancer immunotherapies have had a profound impact on patient care and outcome (3), only a subset of responding patients receive long-term and sustained clinical benefit (4), highlighting the need for new therapeutic approaches.

The PD-1 pathway is comprised of a set of receptors and ligands that are differentially expressed across multiple cell types in the tumor microenvironment (TME). Receptors include PD-1, CD80, and RGMB (repulsive guidance molecule b) and ligands include PD-L1 and PD-L2; interactions among these molecules regulate cells of the adaptive and innate immune system and tumor cells, leading to suppression of immunity (5, 6). The PD-1 receptor is predominantly expressed on subsets of activated T cells and other immune cell types (7) including B cells, natural killer (NK) cells, myeloid cells, and dendritic cells (DC) and binds to both PD-L1 and PD-L2. PD-L1 is generally expressed on activated T cells, antigen-presenting cells (APC; B cells, DCs, and macrophages; ref. 7), across multiple tumors (8), and in some nonimmune cell types like endothelial cells (9). PD-L1 binds to PD-1 and CD80, a shared receptor between PD-L1, CTLA-4 (cytotoxic T-lymphocyte associated protein 4), and CD28. PD-L2 can be present on macrophages and DCs (7); in addition to PD-1, PD-L2 can bind to the RGMB receptor, which has a role in respiratory tolerance in the lung (10). Upon engagement with PD-L1 or PD-L2 ligand, the PD-1 receptor cytoplasmic regions ITIM (immunoreceptor tyrosine-based inhibition motif) and ITSM (immunoreceptor tyrosine-based switch motif) become tyrosine phosphorylated, triggering recruitment of Src homology region 2 domain-containing protein tyrosine phosphatases (SHP-1 and SHP-2) which attenuate T-cell stimulatory signals by dephosphorylating molecules downstream of the T-cell receptor (TCR) and CD28 pathways (11–13). The *cis* interaction of PD-L1 and CD80 on APCs can attenuate PD-L1 to PD-1 suppressive signaling to induce immune response (14–16).

Response rates to both PD-1- and PD-L1–targeting agents are significantly higher in patients with PD-L1–positive tumors (8, 17, 18). However, even in tumors that express high levels of PD-L1, a substantial fraction of patients do not respond to treatment, highlighting the need to improve the activity of these inhibitors. Many combination strategies to inhibit the PD-1 pathway have been clinically evaluated to determine whether they improve cancer patient outcomes, based on the premise that additional pathways and mechanisms are responsible for anti–PD-1 pathway therapy failure. Accordingly, combinations with a broad landscape of immune therapy agents have been evaluated, including other checkpoints, agonist receptors, vaccines, or cell therapies, targeted agents, and chemotherapies (19). These efforts have led to the FDA approval of PD-1 pathway inhibitors combined with anti–CTLA-4 (20, 21) and specific chemotherapy regimens (22–24).

Whereas PD-1 receptors on peripheral T cells are effectively saturated for more than 8 weeks after PD-1 therapy (25, 26), PD-1

Lilly Research Laboratories, Eli Lilly and Company, New York, New York.

Note: Supplementary data for this article are available at Cancer Immunology Research Online (http://cancerimmunolres.aacrjournals.org/).

Corresponding Authors: Helen Kotanides, Eli Lilly and Company, 450 East 29th Street, 12th Floor, New York, NY 10016. Phone: 646-638-5017; E-mail: helen.kotanides@lilly.com, and Michael Kalos, mkalos@arsenalbio.com

Cancer Immunol Res 2020;8:1300–10

doi: 10.1158/2326-6066.CIR-20-0304

receptors on intratumoral T cells remain largely unbound by anti–PD-1 agents (27), suggesting that strategies to develop more effective PD-1 or PD-L1 platform agents might provide benefit to patients. There is a synergistic benefit to PD-1 and PD-L1 combination blockade in mouse tumor model, which associates with enhanced T-cell functionality and antitumor responses to prolong survival (28). There is only one report of a PD-1 and PD-L1 combination human clinical trial (29).

Bispecific antibodies are an attractive approach for dual targeting to generate biological activities normally not possible through monotherapy or drug combinations (30). Bispecific antibodies can enhance efficacy, improve specificity, and induce unique biology through cell bridging all of which can contribute to improved therapeutic outcomes. Bispecific molecules also come with challenges, including issues with stability and expression, and potential dosing and safety concerns associated with cotargeting of distinct biological pathways. The promise of bispecific agents is exemplified principally through the development of CD3 bispecific molecules, which bridge activated T cells to tumor cells (31, 32). There are also multiple rationally designed tumor-targeted and dual-targeted immune checkpoint bispecific molecules that aim to provide superior activity relative to combinations. Clinical trials are testing a number of immune checkpoint bispecifics, including HER2xCD137, PD-1xCTLA-4, and PD-1xLAG3 (lymphocyte activation gene-3; refs. 31, 32), and a bifunctional fusion protein (bintrafusp alfa), composed of a PD-L1 antibody and TGFβ receptor II fusion "trap" (33).

Here, we describe the discovery and preclinical characterization of LY3434172, a human IgG1 mAb with ablated Fc immune effector function that cotargets PD-1 and PD-L1. We hypothesized that a bispecific antibody that simultaneously blocked both PD-1 and PD-L1 could result in more complete inhibition of the PD-1 pathway and facilitate bridging between PD-1–positive activated T cells and PD-L1–positive tumor cells in the TME. One arm of LY3434172 blocks the binding of PD-1 to PD-L1 and PD-L2, while the other arm blocks the binding of PD-L1 to PD-1 and the agonist receptor, CD80. We demonstrated that *in vitro* administration of LY3434172 resulted in enhanced T-cell activation and facilitated bridging of PD-1– and PD-L1–expressing cells. In established human xenograft models reconstituted with human T cells, LY3434172 therapy resulted in robust antitumor activity at doses substantially lower than either parent antibody or their combination. These findings suggested that cotargeting of PD-1 and PD-L1 in a single molecule provides a potent approach to blocking the PD-1 pathway. Collectively, the biological properties and enhanced potency of LY3434172 warrant its clinical development.

Materials and Methods

Cell lines

CHO-K1, HEK-293, WIL2-S, HEL 92.1.7, HCC827, and NCI-H292 cell lines were obtained from ATCC. OV79.FFLuc-2A-gfp was provided by Carl June (University of Pennsylvania, Philadelphia, PA). CHO-K1 cells expressing either human PD-1 or PD-L1 were from Eli Lilly and Company. aAPC/CHO-K1 cells (CS187110) and human PD-L1–positive aAPC/CHO-K1 cells (CS187108) were from Promega. PD-L1 and PD-L2 or CD80 double-positive CHO-K1 cells were generated by lentiviral transduction of PD-L1 aAPC/CHO-K1 with full-length human PD-L2 or by lipofectamine transfection with full-length human CD80 and cultured in F12 supplemented with 10% FBS, 200 μg/mL hygromycin B, 250 μg/mL G418, and 15 μg/mL puromycin. Expression was confirmed by Flow Cytometry (BD Biosciences; anti–PD-L2, 558066 and anti-CD80, 557227). CHO-TCRact-PDL1-scarlet-clone-16 cells were generated by transduction of CHO-TCRact cells (Promega J1191: aAPC/CHO-K1) with virus from pLVX-PDL1-mScarlet lentiviral vector (synthesized by GenScript) and cultured in F12 supplemented with 10% FBS, 200 μg/mL hygromycin B, and 500 μg/mL G418. Jurkat-NFAT-PD1-neonGreen.clone11 suspension cells were generated by transduction of Jurkat-NFAT cells (Promega CS176401) with virus from LVX-PD1-mNeonGreen lentiviral vector (synthesized by GenScript) and cultured in RPMI1640 supplemented with 10% FBS, 200 μg/mL hygromycin B, 500 μg/mL G418, 1 mmol/L sodium pyruvate, and 0.1 mmol/L minimum essential medium non-essential amino acids. Polybrene (Sigma-Aldrich; TR-1003) was used for lentiviral transduction according to the manufacturer's instructions. Expression was confirmed by flow cytometry (anti–PD-1 LY3342903 and anti–PD-L1 LY3300054). U2OS cells coexpressing PD-1 fused to ProLink and PD-L1 fused to enzyme acceptor were generated by DiscoverX and cultured in AssayComplete Cell Culture Kit-103 (DiscoverX) supplemented with 250 μg/mL hygromycin B and 500 μg/mL G418. All cell lines were kept in cell culture for up to 1 month. Cells were not authenticated in the past year. Testing for *Mycoplasma* was regularly performed on stable cell lines using the Lonza MycoAlert Kit (LT07-418).

Antibodies

The PD-1/PD-L1 bispecific antibody, LY3434172 (WO2019014091, Supplementary Fig. S1), was constructed as a human IgG1 heteromab using the Zymeworks Azymetric Bispecific Technology (34). LY3434172 is comprised of a PD-1 monovalent arm derived from LY3342903 (US10316089; ref. 35) and a PD-L1 monovalent arm derived from LY3300054 (US10214586; ref. 36) in an IgG1 Fc effector–null backbone. The heavy and light chain antibody gene sequences were cloned into a mammalian expression vector, expressed in CHO cells, and the protein was purified by Protein A Chromatography (POROS A; Life Technologies). The parent anti–PD-1 and anti–PD-L1 antibodies were produced in a similar manner using HEK-293 cells.

Binding ELISA

PD-1-HIS (Sino Biological, R&D Systems) or PD-L1-HIS (R&D Systems) was coated onto a 96-well plate in PBS overnight at 4°C. The plate was washed and blocked for 2 hours in buffer (1% BSA/PBS) at room temperature. All test antibodies were serially diluted, added to the plate in duplicate, and incubated for 1 hour at room temperature. After washing, goat anti-human IgG $F(ab')_2$-HRP conjugate (Jackson ImmunoResearch Laboratories; 109-035-097) was added and incubated at room temperature for 1 hour. Plates were washed and signal was developed using 3,3′, 5,5′-Tetra-methylbenzidine (TMB) substrate solution from KPL (50-76-00) according to the manufacturer's instructions. Absorbance at 450 nm was read on a Molecular Devices SpectraMax M5e with SoftMax Pro software and the half maximal effective concentration (EC_{50}) was calculated using GraphPad Prism.

Blocking ELISA

For the blocking assay, varying amounts of LY3434172, anti–PD-1, or control IgG were mixed with a fixed amount of biotinylated PD-1-Fc (R&D Systems; 1086-PD), 200 ng/mL for PD-L1 blocking and 100 ng/mL for PD-L2 blocking, and incubated at room temperature for 1 hour. The mixture was transferred in duplicate to 96-well plates precoated with 100 ng/well PD-L1-Fc or PD-L2-Fc (R&D Systems) and then incubated at room temperature for an additional 1 hour. After washing, streptavidin-HRP conjugate (Jackson ImmunoResearch Laboratories; 016-030-084) was added for 1 hour as per the manufacturer's instructions, plates washed and

incubated with TMB (KPL), and absorbance at 450 nm was measured on a SpectraMax M5e with SoftMax Pro Software (Molecular Devices). A similar protocol was used for PD-L1/CD80 blocking assay, except plates were coated with 100 ng/well CD80-Fc (R&D Systems; 140-B1-100) and 500 ng/mL biotinylated PD-L1-Fc was incubated with LY3434172, anti–PD-L1 antibody, or control IgG. The antibody concentration required for 50% inhibition (IC_{50}) of PD-1 binding to PD-L1 or PD-L2 and PD-L1 binding to CD80 was calculated from mean ± SD values using sigmoidal dose response (variable slope) in GraphPad Prism.

Biacore binding

Surface plasmon resonance with a BIACORE T200 Biosensor (GE Healthcare) was used to determine the binding kinetics of LY3434172 to recombinant extracellular human, cynomolgus monkey, mouse, and rat PD-1 and PD-L1 proteins (R&D Systems, Eli Lilly and Company). Anti–PD-1 and anti–PD-L1 antibodies were utilized as positive controls. Antibodies were captured onto a sensor chip CM5 preimmobilized with human Fab Binder (GE Healthcare; 28958325). Soluble PD-L1-Fc or PD-1-His were prepared at concentrations ranging from 0.041 to 30 nmol/L or 0.123 to 90 nmol/L in HBS-EP+ Buffer (GE Healthcare; BR100669) and binding was performed at 37°C. Sample injection was for 180 seconds (contact time) at a flow rate of 30 μL/minute. The dissociation time was 720 seconds followed by regeneration of surface with 10 mmol/L glycine-HCL for 30 seconds (3 to 4 lower concentrations) or 60 seconds (2 to 3 higher concentrations) at a flow rate of 30 μL/minute. Sensorgrams were obtained at each concentration and evaluated using the BIACORE T200 Evaluation Software to determine association (k_{on}) and dissociation (k_{off}) rate constants. The equilibrium dissociation constant (K_D) was calculated from the ratio of rate constants k_{off}/k_{on}.

Flow cytometry

CHO-K1 cells expressing either human PD-1 or PD-L1 were stained in duplicate with Live Dead Zombie Green Viability Dye (BioLegend; 77476) according to the manufacturer's instructions. After washing, cells were blocked with 1× DPBS/1% BSA/0.2 mg/mL purified Human Gamma Globulin (MP Biomedicals; 55838)/0.09% sodium azide and incubated with AF647-conjugated LY3434172, anti–PD-1, anti–PD-L1, or human IgG for 1 hour. Stained cells were acquired on a ZE5 Cell Analyzer (Bio-Rad) and data analyzed using FlowJo Software (Tree Star). Flow cytometry gating strategy and representative plots are provided in Supplementary Fig. S2A and S2B. Median fluorescence intensity (MFI) values were plotted against the concentration of staining antibody and EC_{50} was calculated using a log agonist versus response–variable slope (four parameter) in GraphPad Prism.

Effector function assays

Antibody binding to recombinant human Fcγ receptors (FcγR) was performed in MSD Assay Format (Meso Scale Diagnostics). Briefly, FcγRs were coated onto MULTI-ARRAY standard plate (L15XA) overnight at 4°C, blocked with MSD blocker A (R93BA) for 1 hour at room temperature, and serially diluted test antibodies were added and incubated for 2 hours. Signal was detected with SULFO-TAG Human Secondary Antibody (Meso Scale Diagnostics; D20TF) and the plate developed with MSD Read Buffer T (R92TC). Electrochemiluminescence was measured on the Sector Imager 2400 (Meso Scale Diagnostics). For binding to C1q, test antibodies were serially diluted and coated onto polystyrene ELISA plate overnight at 4°C. Human C1q in casein buffer was added at 0.5 μg/well and incubated for 2 hours at room temperature. Signal was detected with sheep anti-human C1q antibody-HRP (AbD Serotec Inc; 2221-5004P) and developed using TMB. Absorbance was measured at 450 nm with a Synergy Neo2 and Gen5 Software (BioTek). All data analysis and EC_{50} calculation were done with GraphPad Prism.

For antibody-dependent cellular cytotoxicity (ADCC) assay, PD-L1– or PD-1–expressing CHO-K1 or CHO-K1 cells were plated in a 96-well plate at 5×10^3 cells/well in 100 μL of cell growth medium (F12 supplemented with 10% FBS, 250 μg/mL G418, and 200 μg/mL hygromycin B; RPMI supplemented with 10% FBS and 1 mg/mL G418; and F12 supplemented with 10% FBS and 200 μg/mL hygromycin, respectively). After an overnight incubation at 37°C, 50 μL ADCC assay buffer (RPMI1640 with 0.5% BSA) was added and test antibodies and controls were added to target cells at indicated concentrations for 30 minutes. FcγRIIIa-positive Jurkat cells containing NFAT Luciferase Reporter (Eli Lilly and Company) were added to target cells (1.5×10^5 cells/well) and incubated for 6 hours at 37°C. Luminescence signal was measured using Bio-Glo Reagent (Promega, G7940) and microplate reader and the EC_{50} values were calculated using GraphPad Prism Software. The ADCC effector function assay with CD20-positive WIL2-S cells and anti-CD20 antibody, rituximab (IgG1 effector competent) as positive control was performed as described above with cells plated at 1×10^4 cells/well.

For the complement-dependent cytotoxicity (CDC) assay, PD-L1 or PD-1 CHO-K1 or CHO-K1 cells (2.5×10^4 cells/well) and CD20-positive WIL2-S cells (5.0×10^4 cells/well) were seeded in 96-well plates in CDC assay buffer. Test and control antibodies were added in duplicate and incubated for 30 minutes. Human complement (50 μL of 1:5 dilution; Sigma; S1764) was added for 1 hour. AlamarBlue Reagent (Invitrogen; DAL1100) was added to each well for 23 hours. Fluorescence at 560 nm was read on a Synergy Neo2 using Gen5 Software (BioTek) and the EC_{50} calculated with GraphPad Prism Software.

NFAT luciferase reporter assay

PD-L1–negative aAPC/CHO-K1, PD-L1–positive aAPC/CHO-K1, and the PD-L1 and PD-L2 double-positive CHO-K1 cells were plated in a 96-well plate (4.0×10^4 cells/well, F12 media with 10% FBS, 0.2 mg/mL hygromycin-B, and 0.2 mg/mL G418). After overnight incubation at 37°C, serially diluted antibodies (concentration of each antibody tested individually) were added to the wells followed by GloResponse NFAT-luc2/PD1 Jurkat cells (Promega CS187102) at 5.0×10^4 cells/well. After 6-hour induction at 37°C, Bio-Glo Reagent (Promega; G7941) prepared according to the manufacturer's instructions was added and luminescence measured in a SpectraMax M5e with SoftMax Pro Software (Molecular Devices). Data were analyzed and EC_{50} was calculated from mean ± SD using log agonist versus response–variable slope (four parameter) in GraphPad Prism.

Mixed leukocyte reaction

Monocytes were isolated from frozen normal peripheral blood mononuclear cells (PBMC) purchased from AllCells (PB005F) using Monocyte Isolation Kit (Miltenyi Biotec; 130-091-153). Immature DCs were generated by culturing the monocytes in RPMI1640 medium with 10% FBS, 1,000 IU/mL GM-CSF (R&D Systems), and 500 IU/mL IL4 (R&D Systems) for 3 days. Human CD4 T cells isolated from a different PBMC donor (AllCells; PB002) using Human CD4 T Cell Isolation Kit (Miltenyi Biotec; 130-096-533) were cocultured with the DCs in a 96-well plate and antibodies were added. A range of antibody concentrations was tested; human IgG (10.7 nmol/L), anti–PD-1 LY3342903, or anti–PD-L1 LY3300054 (1:3 titration starting at 10.7 nmol/L), and the combination of anti–PD-1 and anti–PD-L1 (1:3

titration starting at 10.7 nmol/L each) or bispecific antibody LY3434172 (1:3 titration starting at 21 nmol/L), each concentration was tested in eight replicates. After incubating the coculture for 66 hours, cell supernatants were measured for secreted INFγ levels in ELISA (R&D Systems; SIF050) using SpectraMax M5 and SoftMax Pro Software (Molecular Devices). EC_{50} was calculated using log agonist versus response (three parameters) in GraphPad Prism.

Tumor cell line killing

DCs were generated as described above for mixed lymphocyte reaction (MLR) assay (except culturing was for 2 days). Pan T cells were isolated from fresh human PBMCs (AllCells; PB002) of another donor using Pan T Cell Isolation Kit (Miltenyi Biotec; 130-096-535). DCs (5×10^3 cells/well) were mixed with pan T cells (5×10^4 cells/well) in AIM-V medium, plated onto a 96-well plate, and then serially diluted control or test antibodies (1:3 starting at 6 nmol/L, combination at 3 nmol/L each) were added (eight replicates). After 48-hour coculture, 2.5×10^4 human erythroleukemia HEL 92.1.7 cells labeled with CellTrace Violet (Invitrogen; C34571) according to the manufacturer's instructions were added to each well and incubated for 12 hours; the identity of target antigen(s) on HEL cells was undefined. Cells were pooled for each treatment, costained with 7-AAD (eBioscience), and data were acquired on LSRFortessa X-20 Flow Cytometer (BD Biosciences) and analyzed using FlowJo. Flow cytometry gating strategy is provided in Supplementary Fig. S2C. Briefly, total HEL tumor cells were first gated on the basis of CellTrace Violet staining. The percentage of viable HEL cells (7-AAD–negative population) and nonviable HEL cells (100 − % viable cells) was analyzed and EC_{50} determined using log agonist versus response (three parameters) in GraphPad Prism.

Receptor association

To measure PD-1 and PD-L1 interactions, a β-galactosidase (β-Gal) Enzyme Fragment Complementation (EFC) Assay was used (DiscoverX). Briefly, U2OS cells coexpressing PD-1 fused at its carboxy terminus to the small enzyme fragment, ProLink and PD-L1 fused at its carboxy terminus to the larger enzyme fragment, enzyme acceptor, were plated at 5×10^3 cells/well in 384-well plates. LY3434172, anti–PD-1, anti–PD-L1, and control IgG (diluted 2-fold, starting at 100 nmol/L each) were added to the cells and incubated for 16 hours. PathHunter Flash Detection Reagent (DiscoverX; 93-0247) was added to plate and incubated for 1 hour at room temperature. Luminescence was measured on a Synergy Neo2 Microplate Reader with Gen5 Software (BioTek) and data were plotted in GraphPad Prism.

Cell bridging

PD-1- or PD-L1–expressing CHO-K1 cells were nonenzymatically dissociated. PD-L1 CHO cells were stained red with CellTracker DeepRed CTDR (Thermo Fisher Scientific; C34565) following the manufacturer's standard method, while PD-1 CHO cells were stained with CFSE (BD Horizon; 565082) using a modified method that included the addition of 5% FCS and carboxyfluorescein diacetate succinimidyl ester (CFSE) at 3 μmol/L. After staining, cells were washed and resuspended in Assay Buffer [PBS + 1% BSA-sulfhydryl blocked (Lee Bio) + 0.09% Sodium Azide (Sigma)]. Labeled PD-1 CHO and PD-L1 CHO cells were each incubated for 2 hours on ice with titrated LY3434172. Separately on ice, PD-L1 CHO cells were incubated for 2 hours with 45 μg/mL of anti–PD-L1 or hIgG1 control and PD-1 CHO cells were incubated for 2 hours with 45 μg/mL of anti–PD-1 or hIgG4 control. PD-1 CHO + LY3434172 were mixed with PD-L1 CHO + anti–PD-L1 or IgG1 control and PD-L1 CHO + LY3434172 were mixed with PD-1 CHO + anti–PD-1 or IgG4 control, all at a ratio of 1:5. After incubating for 72 hours at 4°C, samples were evaluated on LSRFortessa X20 (BD Biosciences). FlowJo software was used to gate $CFSE^+/CTDR^-$, $CFSE^-/CTDR^+$, and $CFSE^+/CTDR^+$ events. Flow cytometry gating strategy and representative plots are provided in Supplementary Fig. S2D. Data were plotted using GraphPad Prism.

Confocal microscopy and live cell imaging

The live cell imaging studies were conducted within multi-well plates and run on a Nikon A1R Confocal Microscope (Nikon Instruments) equipped with environmental controls. Imaging was conducted over several hours with multipoint image acquisition occurring every minute allowing all experimental conditions to be collected in the same study. Following acquisition, image sequences were analyzed in Nikon Elements (Nikon Instruments) to quantify PD-1 localization to the immune synapse, and image stills and movies were exported to generate figures.

CHO-TCRact-PDL1 cells and CHO-TCRact-PDL1-scarlet-clone-16 cells were seeded into PerkinElmer CellCarrier 96-well plates at 1.5×10^4 cells/well (100 μL volume). Jurkat-NFAT-PD1-neonGreen.clone11 suspension cells were combined (3×10^4 cells, 50 μL volume) with antibodies (10 μg/mL of unlabeled or Alexa-647 fluorescently labeled LY3434172, anti–PD-1, anti–PD-L1, or control IgG) and added directly to the wells during the live cell imaging run. Cells were allowed to equilibrate in the live-cell imaging chamber for 30 minutes, the imaging parameters were established, and the run initiated; Jurkat cell with antibody mixture was added and the time lapse conducted.

The Nikon-A1R Confocal Microscope was equipped with a 20 × (NA 0.65) air or 60 × (NA1.40) oil objective in a live-cell imaging chamber heated to 37°C and containing humidified 5% CO_2. Three fields were captured for each well, with acquisition every 1 minute for 60 minutes. Quantitation of Jurkat cells containing PD1-neonGreen localized to immune synapse was performed at the 60 minute timepoint by dividing the number of PD-1 Jurkat cells containing PD1-neonGreen enriched at the immune synapse by the total number of PD-1 Jurkat cells bound to generate the % PD-1 Jurkat cells with PD1-neonGreen localized to the immune synapse. Data were imported into GraphPad Prism for analysis. Using Nikon-Elements, movies were generated from the Nikon ND2 files and exported as .avi files, stamped with time parameters and scale bar, imported into ImageJ (Fiji), and compressed to .mov files. In addition, still images were captured in Nikon-Elements and exported as TIFF files to depict time lapse sequences.

Animal *in vivo* efficacy studies and models

Humanized mouse tumor models were performed as described previously (36). All animal research methods and studies were approved by the Institutional Animal Care and Use Committee and performed in accordance with current regulations and standards of the U.S. Department of Agriculture and the NIH. Female NOD/SCID Gamma (NSG) mice at 7 weeks age (Jackson Laboratories) were used for all *in vivo* studies. Mice were housed in a 12-hour light/dark cycle facility under pathogen-free conditions in microisolator cages with standard laboratory chow and water *ad libitum*. Body weight and tumor volume were measured twice weekly. Tumor volume was calculated using the formula [tumor volume (mm^3) = $\pi/6 \times$ length $\times$ width^2) and plotted as geometric means ± SEM. The %T/C (ratio between the tumor volume in the treated group and in the control group) was calculated by the formula $100 \times \Delta T/\Delta C$, if $\Delta T > 0$ of the

geometric mean values. ΔT, mean tumor volume of the drug-treated group on the observation day of the study − mean tumor volume of the drug-treated group on initial day of dosing; ΔC, mean tumor volume of the control group on the observation day of the study − mean tumor volume of the control group on initial day of dosing. Regression was calculated using the formula = $100 \times \Delta T/T_{initial}$, if $\Delta T < 0$. Animals with <14 mm^3 tumor volume for three consecutive measurements were considered as complete responders and tumors with >50% regressions were partial responders. The % change in body weight was calculated by the formula (body weight on observation day − body weight on initial day)/body weight on initial day × 100%.

For the established tumor model, HCC827 human non–small cell lung cancer (NSCLC) cells were injected subcutaneously into right flank of mice (10×10^6 cells, 200 μL/mouse in Hank's Balanced Salt Solution). When tumors reached approximately 250–400 mm^3 in size, mice were randomized into groups and human expanded T cells (3×10^6 cells, 200 μL/mouse in DPBS) injected intravenously by tail vein. As a control, tumor cells alone were implanted with no T cells. Treatment groups were all dosed intraperitoneally at indicated doses (10 μL/g body weight in PBS). Tumor volumes were measured twice per week using electronic calipers. The established OV79 human ovarian tumor model was performed similarly, except tumor cells (5×10^6 OV79.FFLuc-2A-gfp) were implanted subcutaneously into the flanks of NSG mice (37) and when tumor volumes reached 600–700 mm^3, they were dissected into smaller fragments (4–5 mm in diameter) and passaged to NSG mice (subcutaneously implanted fragments). Expanded human T cells were infused (10×10^6 cells) when tumors reached 200–250 mm^3 and treatments dosed interperitoneally as indicated. T cells were expanded with Dynabeads Human T-Expander CD3/CD28 Beads (Thermo Fisher Scientific; 11141D) for 10 days.

In the preventative model, freshly isolated human PBMCs from whole blood were combined with freshly cultured NCI-H292 human NSCLC tumor cells at a 1:4 ratio of PBMCs to tumor cells (0.5×10^6 PBMC and 2×10^6 NCI-H292 cells) and implanted subcutaneously on the right flank of NSG mice with 0.2 mL of the solution on day 0. A control group receiving tumor cells alone was included. Mice were randomly assigned to treatment groups and dosed intraperitoneally as indicated. Tumor volumes were measured twice per week using electronic calipers.

In vivo pharmacokinetic studies

The pharmacokinetic (PK) study in female SCID mice was conducted at Covance and approved by the Institutional Animal Care and Use Committee. Twelve female SCID mice (CB17/Icr-Prkdcscid/IcrIcoCrl) from Charles River Laboratories were given a single intravenous dose of 10 mg/kg of LY3434172 (0.1 mL solution in PBS) via the tail vein. Blood (∼0.2 mL) was collected from 3 animals/group/timepoint at 0.25, 6, 24, and 72 hours after dose via submandibular puncture. Blood was collected from 3 animals/group/timepoint at 168, 336, 504, and 672 hours after dose via cardiac puncture under isoflurane anesthesia. Following each collection, blood was transferred into tubes containing no anticoagulant (serum separator tubes) and samples were allowed to clot under ambient conditions prior to centrifugation to obtain serum. Sera samples were stored at approximately −70°C.

Bioanalysis of serum samples from PK study

Serum samples were analyzed for LY3434172 concentrations using three ELISA methods (total IgG, PD-1 antigen capture, and PD-L1 antigen capture). The total IgG ELISA method utilized a goat anti-human IgG $F(ab')_2$ antibody (Jackson ImmunoResearch Laboratories) as the capture reagent and a mouse anti-human IgG-Fc conjugated to horseradish peroxidase (HRP, Southern Biotech) as the detection reagent. Total IgG ELISA had the lower limit of quantitation (LLOQ) of 45 ng/mL and the upper limit of quantitation (ULOQ) of 375 ng/mL. For PD-1 and PD-L1 antigen capture ELISA methods, LY3434172 in serum samples was captured by immobilized antigen recombinant human PD-1 or PD-L1 Fc Chimeric Protein (R&D Systems), respectively, followed by detection using goat anti-human IgG ($F(ab')_2$ fragment specific) antibody conjugated to HRP (Jackson ImmunoResearch Laboratories). The LLOQ was 6 ng/mL and ULOQ was 45 ng/mL for both methods. PK parameters were estimated using Phoenix WinNonlin Software (Certara) using a noncompartmental approach consistent with the intravenous bolus injection route of administration. All parameters were generated using mean serum LY3434172 concentrations at each timepoint and nominal sampling times relative to the start of each dose administration.

Statistical analysis

Data are shown as the mean ± SD or mean ± SEM as described in the figure legends. All *in vitro* assay statistical analyses were performed using specific tests in GraphPad Prism Software (GraphPad) as indicated in the figure legends. Statistical analysis of tumor volume data was performed with a two-way repeated measures ANOVA by time and treatment using the MIXED procedures in SAS Software (SAS Institute). A Bliss independence analysis was performed to determine whether combination treatment tested was additive or greater than additive or less than additive as compared with either single agent.

Results

Assembly and biophysical properties of LY3434172

The dual PD-1 and PD-L1–targeting bispecific antibody, LY3434172, was generated using the Zymeworks Azymetric Platform (34), a format that allowed for assembly of a human IgG1 bispecific heteromab with two distinct monovalent arms. The anti–PD-1 arm comprised of antibody LY3342903 and the anti–PD-L1 arm with antibody LY3300054 (Supplementary Fig. S1A–S1E). To ensure proper assembly of each cognate light chain to its respective heavy chain, sets of mutations were introduced into the light chain constant region and heavy chain CH1. In addition, an Fc effector–null backbone was introduced into the bispecific by mutagenesis (L234A, L235A, and D265S) to prevent Fc-mediated effector function. The binding specificity and affinity of each arm of LY3434172 were evaluated relative to the corresponding parent antibody in binding ELISA against immobilized human PD-1 and human PD-L1 proteins; these analyses demonstrated similar binding affinities of each monovalent arm relative to the parent antibodies (PD-1 EC_{50}: parent = 0.132 nmol/L, bispecific = 0.080 nmol/L and PD-L1 EC_{50}: parent = 0.475 nmol/L, bispecific = 0.455 nmol/L; Supplementary Fig. S3A). Binding kinetics of LY3434172 for PD-1 and PD-L1 proteins were measured using Biacore (**Table 1**); these analyses demonstrated high affinity binding by each monovalent arm, with both PD-1 and PD-L1 arms retaining similar affinity to the parent bivalent monoclonals.

Species cross-reactivity of LY3434172 was observed against cynomolgus monkey PD-1 and PD-L1, but not to mouse or rat in the binding assays (**Table 1**; Supplementary Fig. S3B). The ability of LY3434172 to fully block receptor–ligand interactions in the PD-1 pathway was examined by ELISA assays using

Table 1. Binding kinetics and cross-reactivity to PD-1 and PD-L1 by Biacore.

Antibody	Analyte	k_{on} (1/Ms)	k_{off} (1/s)	K_D (M)
LY3434172	PD-1 human	4.77E+05	2.10E-04	4.41E-10
	PD-1 cyno	4.64E+05	1.30E-04	2.80E-10
	PD-1 rat	N.B.	N.B.	N.B.
	PD-1 mouse	N.B.	N.B.	N.B.
	PD-L1 human	2.69E+06	1.50E-03	5.60E-10
	PD-L1 cyno	2.81E+06	1.65E-03	5.88E-10
	PD-L1 rat	N.B.	N.B.	N.B.
	PD-L1 mouse	N.B.	N.B.	N.B.
LY3342903 anti–PD-1	PD-1 human	5.35E+05	2.00E-04	3.74E-10
	PD-1 cyno	4.96E+05	1.28E-04	2.58E-10
LY3300054 anti–PD-L1	PD-L1 human	2.44E+06	3.20E-04	1.31E-10
	PD-L1 cyno	2.83E+06	2.36E-04	8.33E-11

Abbreviations: cyno, cynomolgus monkey; M, mol/L; N.B., no detectable binding.

recombinant PD-1, PD-L1, PD-L2, and CD80 proteins as shown (Supplementary Fig. S3C). LY3434172 inhibited binding of PD-1 to both PD-L1 (slight bell-shaped curve may represent ligand to receptor bridging signal) and PD-L2 (IC_{50} = 2.27 nmol/L), and also blocked the binding of PD-L1 to CD80 (IC_{50} = 0.75 nmol/L).

Functional activity of LY3434172 in cell-based assays

The functional activity of LY3434172 to bind and block the PD-1 pathway and enhance T-cell activity was assessed *in vitro* by cell-based assays. Specific binding of LY3434172 to PD-1- or PD-L1–expressing cells was evaluated using flow cytometry and CHO cells engineered to express each target; these experiments demonstrated specific binding of LY3434172 to each target and also that the binding affinity of LY3434172 for each target was largely preserved (within 3- to 4-fold) relative to the parental antibodies (PD-1 EC_{50}: parent = 0.808 nmol/L, bispecific = 2.39 nmol/L and PD-L1 EC_{50}: parent = 0.146 nmol/L, bispecific = 0.589 nmol/L; **Fig. 1A**; Supplementary Fig. S2B). The Fc effector function of LY3434172, engineered as an IgG1 effector–null

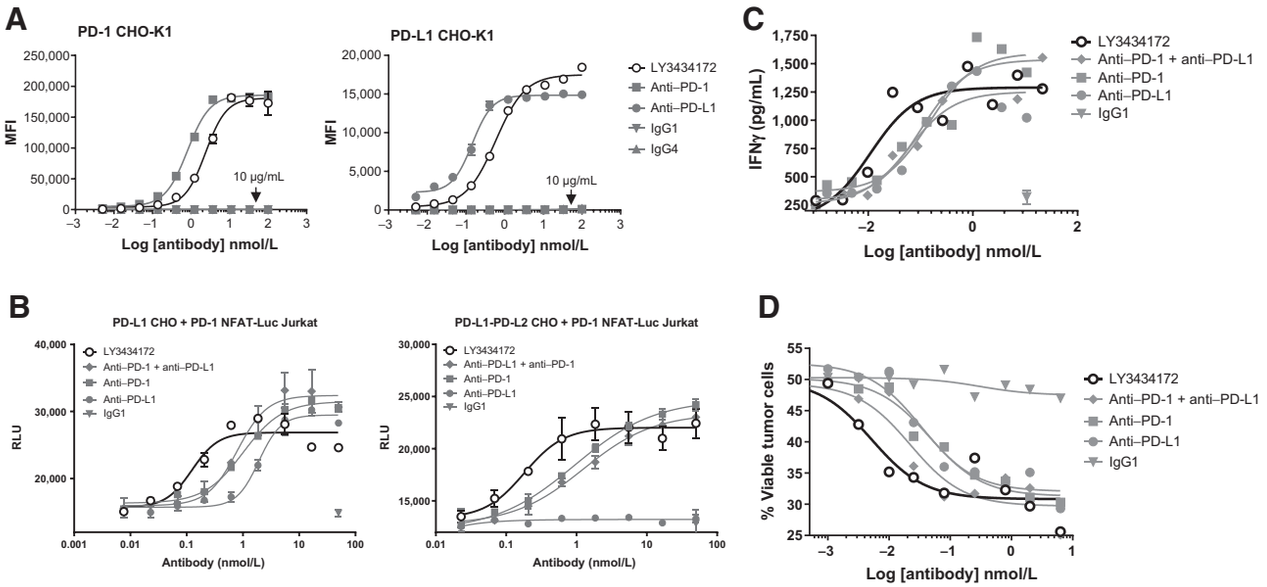

Figure 1.

Functional activity of LY3434172 *in vitro*. **A,** Binding of LY3434172 to CHO-K1 cells expressing cell-surface PD-1 or PD-L1 by flow cytometry. The mean fluorescence intensity (MFI) of each concentration point (two replicates) is shown. **B,** NFAT reporter assay. Increasing concentrations of LY3434172, anti–PD-1, anti–PD-L1, or the antibody combination and control IgG were added to PD-L1 aAPC/CHO-K1 or PD-L1 and PD-L2 aAPC/CHO-K1 cells, followed by NFAT-Luc2/PD1 Jurkat effector cells. Luminescence signal is plotted as relative light units (RLU) versus antibody concentration as shown (mean ± SD; $n = 2$). PD-L1 CHO: LY3434172, $P = 0.002$ versus anti–PD-1 + anti–PD-L1, $P = 0.010$ versus anti–PD-1, $P = 0.002$ versus anti–PD-L1. PD-L1 + PD-L2 CHO: LY3434172; $P = 0.007$ versus anti–PD-1 + anti–PD-L1, $P = 0.019$ versus anti–PD-1. Statistical significance was determined by extra sum-of-squares F test. **C,** MLR of allogeneic immature DCs and CD4 T cells in the presence of test antibodies as indicated. IFNγ levels measured by ELISA (mean ± SD; $n = 8$) are shown. LY3434172, $P = 0.038$ versus anti–PD-1 + anti–PD-L1, $P = 0.028$ versus anti–PD-1, $P = 0.009$ versus anti–PD-L1. Statistical significance was determined by extra sum-of-squares F test. **D,** Tumor cell line killing. Human CD4 and CD8 T cells were cocultured with immature DCs and serially diluted antibodies as indicated. The percentage of viable HEL tumor cells (7-AAD stained) is shown in graph. LY3434172, $P = 0.058$ versus anti–PD-1 + anti–PD-L1, $P = 0.002$ versus anti–PD-1, $P = 0.001$ versus anti–PD-L1. Statistical significance determined by extra sum-of-squares F test. **A–D,** Data are from one representative of at least two experiments.

bispecific, was evaluated in the PD-1- and PD-L1–expressing CHO cells; no detectable ADCC activity was observed in response to LY3434172 in the PD-L1 CHO, PD-1 CHO, or CHO parent cells (Supplementary Fig. S4; Supplementary Table S1). No specific binding of LY3434172 to human FcγRs was detected in ELISA (Supplementary Table S2). Finally, LY3434172 showed no activity in CDC assay or binding by ELISA to complement protein C1q (Supplementary Tables S1 and S2).

To evaluate the ability of LY3434172 to functionally block the PD-1 pathway, we employed both NFAT-driven luciferase reporter–based and primary T cell assays. For the reporter-based assays, Jurkat cells expressing PD-1 and NFAT reporter were cocultured with PD-L1 or dual PD-L1 + PD-L2 stable expressing CHO cells in the presence of LY3434172, each individual parent antibody, or their combination; NFAT reporter expression increased significantly in response to LY3434172 treatment relative to the combination or monotherapy in both PD-L1 (EC_{50} = 0.12 vs. 0.80 nmol/L for combination; P = 0.002) and PD-L1 + PD-L2 (EC_{50} = 0.18 vs. 1.25 nmol/L for combination; P = 0.007) expressing cells (**Fig. 1B**). Anti–PD-L1 alone provided no NFAT reporter activity in the dual PD-L1 + PD-L2 CHO cells potentially due to PD-L2–mediated engagement of the PD-1 inhibitory axis. CD80 coexpression on PD-L1 CHO cells had no impact on NFAT reporter signal in these experiments (Supplementary Fig. S5).

The functional activity of LY3434172 was further evaluated in an MLR assay. In this assay, the allogeneic response of primary T cells against allogeneic DCs can be suppressed by blocking the PD-1 pathway (36, 38). As assessed by both cytokine and cytotoxicity measurements, LY3434172 treatment was effective in PD-1 pathway inhibition at approximately 4- to 10-fold lower concentration compared with the combination of each parental antibody, as shown in **Fig. 1C** [EC_{50} = 0.01 vs. combination EC_{50} = 0.10 nmol/L (P = 0.038) or monotherapy EC_{50} (anti–PD-L1 = 0.06 nmol/L and anti–PD-1 = 0.15 nmol/L)] and **Fig. 1D** [EC_{50} = 0.005 vs. combination EC_{50} = 0.022 nmol/L (P = 0.058) or each monotherapy EC_{50} (anti–PD-1 = 0.046 nmol/L and anti–PD-L1 = 0.034 nmol/L)].

LY3434172 induced PD-1 and PD-L1 receptor association and cell-to-cell bridging

The ability of LY3434172 to facilitate cobinding of PD-1 and PD-L1 on cells in *cis* and *trans* was evaluated. A previous report described *cis* interaction of PD-1 and PD-L1 in an FRET assay (39). To measure receptor *cis* interactions in response to LY3434172, we utilized a β-gal EFC assay; and U2OS cells that coexpressed PD-1 fused to the small enzyme fragment and PD-L1 fused to the larger complementary enzyme fragment. Addition of LY3434172 increased the association of the fusion partners resulting in an active β-gal enzyme that

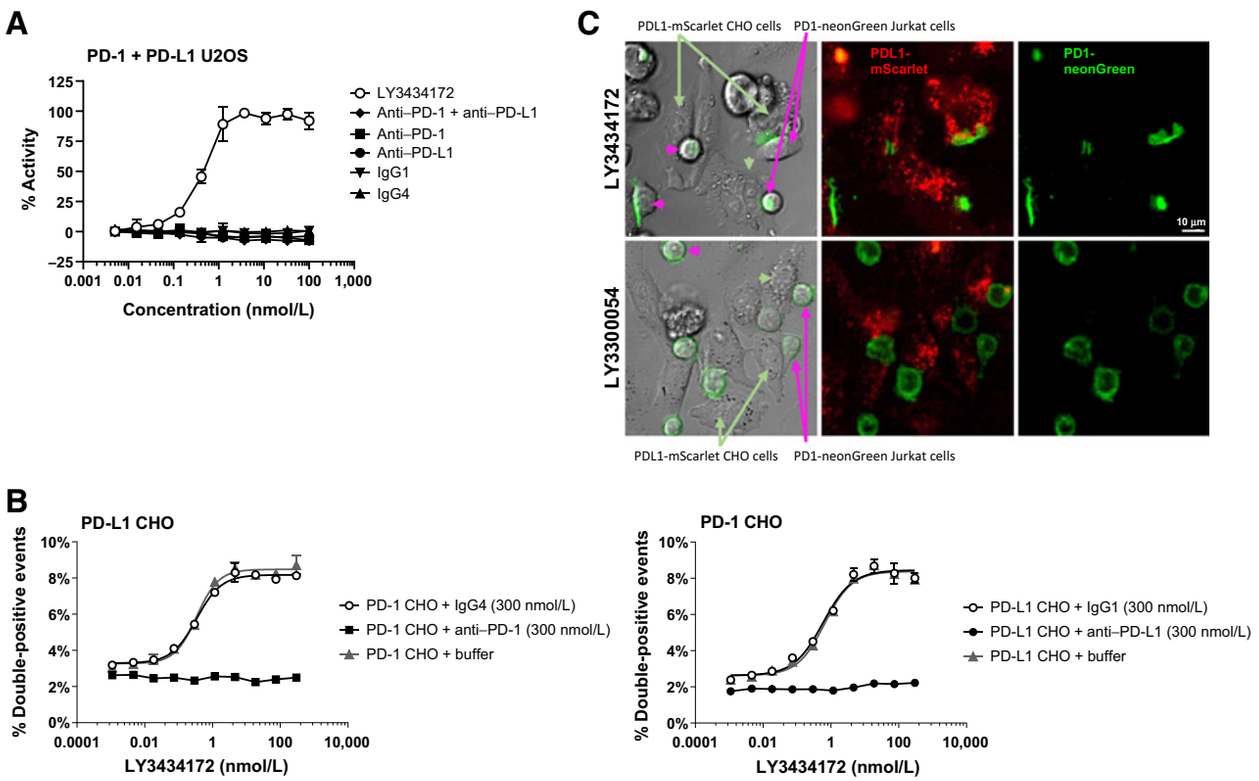

Figure 2.

LY3434172 promoted association of PD-1 and PD-L1 and cell–cell interaction *in vitro*. **A,** PD-1 and PD-L1 receptor association in response to LY3434172 in a β-gal EFC assay. Plotted is the mean ± SD of three replicates. **B,** Bridging of PD-1– and PD-L1–expressing CHO-K1 cells by flow cytometry. Percentage of double-positive events (green PD-1 CHO and red PD-L1 CHO detected by flow cytometry) as a function of LY3434172 concentration is plotted (mean ± SD; n = 2). IgG1 and IgG4 are effector function–null negative controls. **C,** PD1-neonGreen is relocalized to cell–cell contact sites between the PD1 Jurkat (green) and PDL1 CHO (scarlet) cells upon incubation of bispecific LY3434172 (top) but remains evenly distributed in the plasma membrane after anti–PD-L1 LY3300054 addition (bottom). Representative images are shown. Scale bars, 10 μm. **A–C,** Data represent one of at least two experiments.

hydrolyzed substrate to generate a chemiluminescence signal; in contrast, neither the parent antibodies nor their combination resulted in receptor association (**Fig. 2A**) and there was no detectable baseline interaction in this system. To evaluate whether LY3434172 facilitated cell bridging through binding to each receptor in *trans*, we fluorescently labeled PD-1 CHO (green) and PD-L1 CHO (red) cells with different dyes and then treated with the bispecific antibody followed by flow cytometry analysis (Supplementary Fig. S2D); LY3434172 addition induced doublets of PD-L1 CHO and PD-1 CHO cells at levels above baseline, an effect that was abrogated by preincubation with either anti–PD-1 or anti–PD-L1 (**Fig. 2B**).

To further evaluate the cell-to-cell interactions mediated by LY3434172, we employed live-cell confocal microscopy. PDL1-scarlet CHO cells and PD1-neonGreen Jurkat cells were cocultured with LY3434172, anti–PD-L1, or anti–PD-1 and control hIgG followed by live-cell imaging. Whereas baseline cell-to-cell contacts between PDL1-scarlet CHO and PD1-neonGreen Jurkat cells were observed with control hIgG, treatment with the bispecific antibody increased relocalization of PD1-neonGreen at the contact sites (control hIgG = 62%; bispecific = 97%; **Fig. 2C**; Supplementary Fig. S6A and S6B). Treatment with control anti–PD-L1 or anti–PD-1 resulted in a more even distribution of PD1-neonGreen on the plasma membrane (12%–21% at contact sites; Supplementary Fig. S6A and S6B). Using time-lapse imaging in the presence of CHO cells (PDL1-scarlet), a rapid redistribution of PD-1 receptor in Jurkat cells (PD1-neonGreen) at the immune synapse was observed within minutes of LY3434172 treatment (Supplementary Fig. S6C).

Pharmacokinetics of LY3434172 in mice

The serum PK profile of bispecific LY3434172 was characterized in female SCID mice following a single intravenous bolus dose of 10 mg/kg LY3434172 as shown in Supplementary Fig. S7. Collected serum samples provided similar concentrations of LY3434172 in each ELISA assay, suggesting bispecific stability in circulation as reported in Supplementary Table S3. LY3434172 showed a biexponential serum concentration–time profile with a short distribution phase followed by a long elimination phase. LY3434172 PK demonstrated a human IgG–like profile, which was characterized with low clearance (CL) of 0.15 mL/hour/kg (as determined by total IgG ELISA) and long terminal half-life ($t_{1/2}$) of 293 hours. The volume of distribution at steady state (V_{ss}) was 68.1 mL/kg, similar to mouse blood volume.

Antitumor efficacy of LY3434172 in humanized mouse tumor models

The biological activity of LY3434172 was evaluated *in vivo* using humanized tumor xenograft mouse models established as reported previously (36); these models evaluate the ability of a therapeutic intervention to modulate the alloreactivity of an infused human T-cell graft against implanted human PD-L1–expressing tumors. The activity and potency of LY3434172 were evaluated and compared with each parent antibody as well as the combination of both antibodies. In the HCC827 NSCLC human established tumor model, LY3434172 treatment resulted in antitumor efficacy over a broad dose range of 2, 0.2, and 0.02 mg/kg/week (%T/C = 3.9, 19.4, and 50.3, respectively, with $P < 0.001$ for each), with significant antitumor activity observed

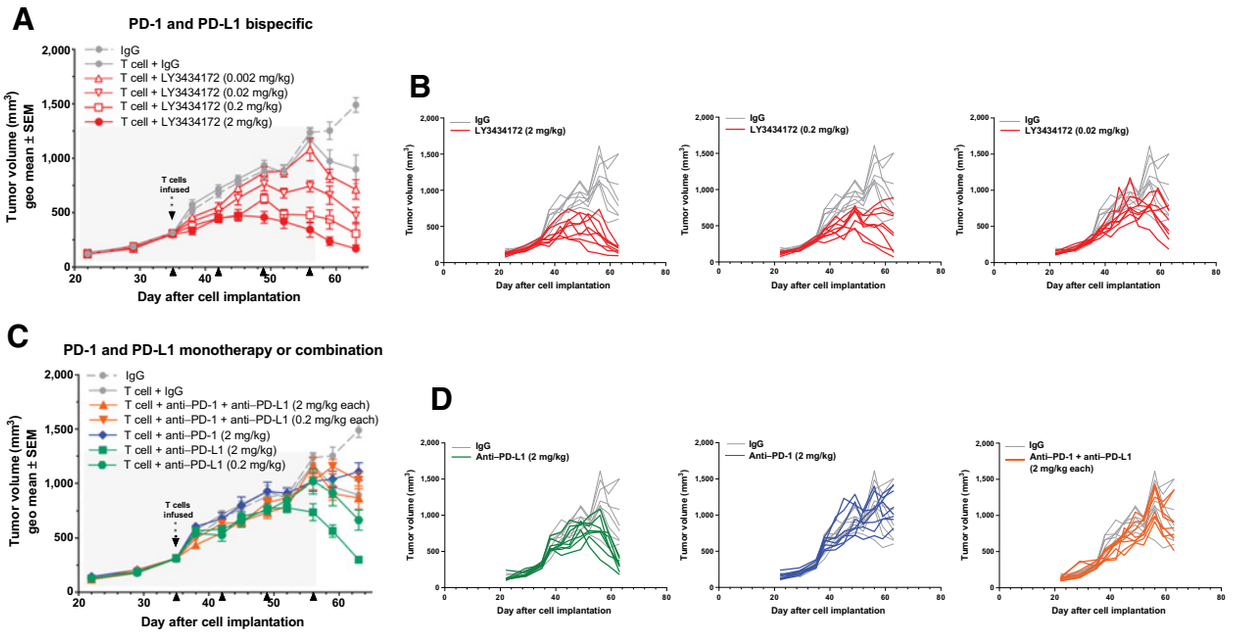

Figure 3.

LY3434172 demonstrated *in vivo* antitumor efficacy in HCC827 human tumor xenograft mouse model reconstituted with human T cells. **A,** HCC827 NSCLC established tumors in NSG mice testing the dose response of bispecific antibody LY3434172 as indicated. Statistically significant tumor volume reduction by LY3434172 at 2, 0.2, and 0.02 mg/kg doses ($P < 0.001$) compared with control IgG. **B,** Graphs of individual animal tumor volumes of LY3434172 compared with IgG control. **C,** Dose response to control parent antibodies, anti–PD-1 and anti–PD-L1, and the combination of both as indicated. Statistically significant tumor volume reduction by control anti–PD-L1 at 2 mg/kg dose ($P < 0.001$) compared with control IgG. **D,** Graphs of individual animal tumor volumes for anti–PD-1, anti–PD-L1, and the combination of both compared with IgG control. **A–D,** Human T cells were infused on day 35, and dosing was once weekly as indicated by arrows; tumor volumes are shown as geometric mean ± SEM, $n = 8$ per group. Statistical testing by two-way repeated measures ANOVA by time and treatment.

even at the low dose of 0.02 mg/kg/week (**Fig. 3A** and **B**). As reported previously (36), the parental anti–PD-L1 was effective in this model at the 2 mg/kg dose (%T/C = 49.7; $P < 0.001$), with no significant activity observed at lower doses (0.2 mg/kg/week: %T/C = 82.4; $P = 0.318$). The activity of the parent antibodies was considerably lower than that of LY3434172 tested at these same doses; neither the anti–PD-1 monotherapy nor the anti–PD-1 and anti–PD-L1 combination therapy showed significant activity at any dose tested (**Fig. 3C** and **D**). LY3434172 treatment at all doses did not result in significant toxicity as assessed by body weight measurements in animals throughout the duration of the study (Supplementary Fig. S8A). In separate studies that evaluated higher doses of antibodies, LY3434172 treatment resulted in enhanced activity compared with either parental antibody in the HCC827 and OV79 established tumor models (Supplementary Fig. S9A and S9B).

The activity of LY3434172 was also examined in a preventative coimplantation tumor model using the NCI-H292 NSCLC cell line. In this model, LY3434172 showed robust antitumor activity (prevention of tumor cell engraftment) and superior activity (**Fig. 4A** and **B**) including complete responses (CR) in a majority of animals treated at 0.25 mg/kg/week (%T/C = 6; $P < 0.001$; 5/8 CRs). Whereas the anti–PD-L1 monotherapy also showed antitumor activity at the 0.25 mg/kg dose (%T/C = 25; $P < 0.001$; 1/8 CRs), LY3434172 was more efficacious relative to anti–PD-L1 ($P = 0.003$) and to the combination of anti–PD-1 and anti–PD-L1 ($P < 0.001$), which provided no benefit (**Fig. 4C** and **D**). Treatment at all doses did not result in significant toxicity as assessed by body weight measurements in animals throughout the duration of the study (Supplementary Fig. S8B). Higher doses of LY3434172 treatment in separate NCI-H292 study also showed enhanced activity compared with parental antibodies (Supplementary Fig. S9C). These results show dual blockade of both PD-1 and PD-L1 by LY3434172 enhances T-cell activation and antitumor immune response.

Discussion

Whereas inhibitory antibodies that target the PD-1 pathway show considerable promise as cancer immunotherapies, significant numbers of patients still fail to achieve a durable response. Some of these therapeutic failures are due to the lack of a potent tumor-specific repertoire and the existence of additional suppressive pathways. Additional explanations could relate to the breadth and complexity of PD-1 pathway receptor and ligand expression in certain subsets of patients or from incomplete PD-1 pathway blockade because

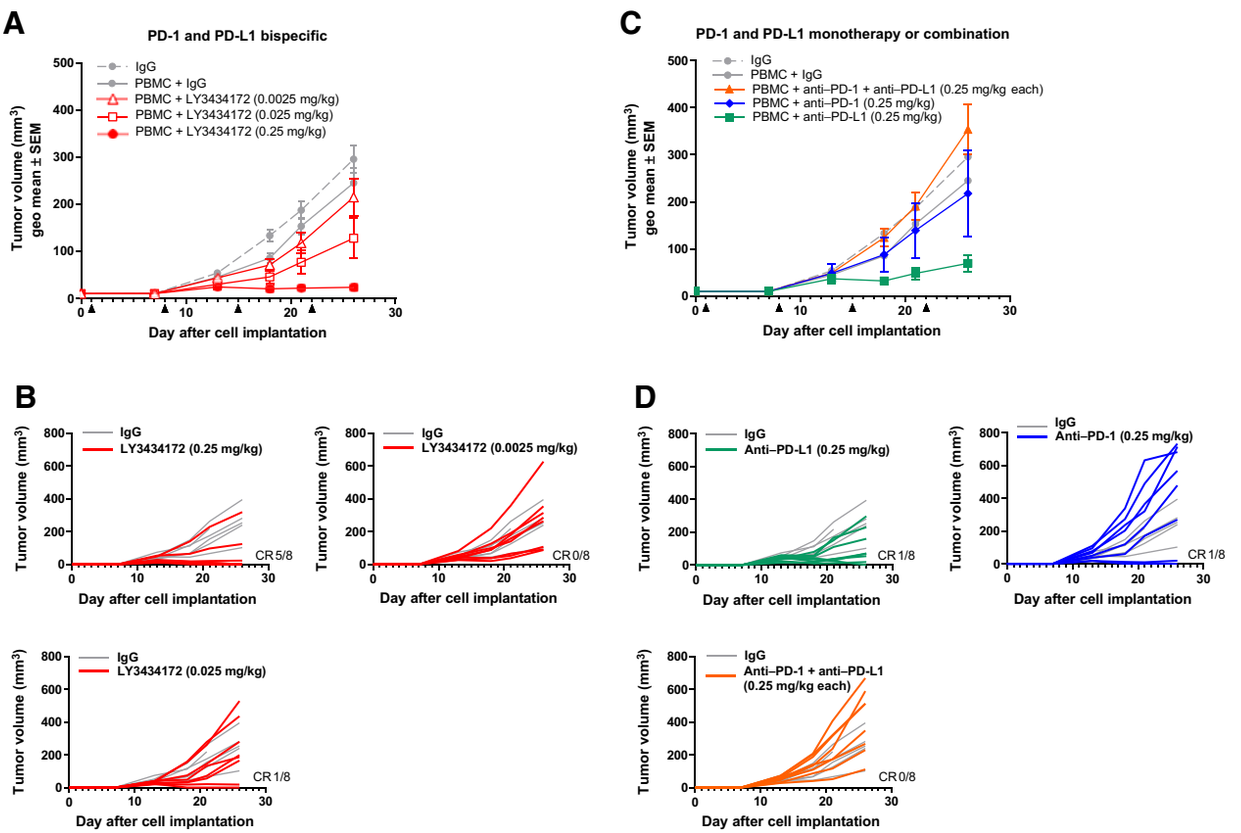

Figure 4.

LY3434172 demonstrated *in vivo* antitumor efficacy in NCI-H292 human tumor xenograft mouse model coimplanted with human PBMCs. **A,** NCI-H292 tumors in NSG mice testing the dose response of bispecific antibody LY3434172 as indicated. Statistically significant tumor volume reduction by LY3434172 at 0.25 mg/kg ($P < 0.001$) compared with IgG. **B,** Graphs of individual animal tumor volumes of LY3434172 compared with IgG control. **C,** Response of control parent antibodies, anti–PD-1 and anti–PD-L1, and the combination of both as indicated. Statistically significant tumor volume reduction by control anti–PD-L1 at 0.25 mg/kg ($P < 0.001$) compared with IgG, LY3434172 compared with anti–PD-L1 ($P = 0.003$), or the anti–PD-1 and anti–PD-L1 combination ($P < 0.001$). **D,** Graphs of individual animal tumor volumes of anti–PD-1, anti–PD-L1, and the combination of both compared with IgG control. **A–D,** Tumor cells and PBMCs were coimplanted on day 0, and dosing was once weekly as indicated by arrows; tumor volumes are shown as geometric mean ± SEM, $n = 8$ per group. Statistical testing by two-way repeated measures ANOVA by time and treatment.

of unchecked CD80 or CTLA-4 agonism. Here, we described the development and preclinical characterization of LY3434172, a first-in-class bispecific antibody that simultaneously blocks both the PD-1 and PD-L1 molecules to more completely block inhibitory interactions between PD-1 pathway molecules. Whereas bispecific antibodies with anti–PD-1 or anti–PD-L1 arms have been described (31, 32), to date, there is limited information on combinations of anti–PD-1 and anti–PD-L1 agents (29).

We hypothesized that a more comprehensive blockade of the PD-1 pathway mediated through a bispecific molecule that also bridged PD-1–expressing T cells and PD-L1–expressing tumor cells would result in enhanced effector T-cell activation and tumor cell killing relative to parent anti–PD-1 or anti–PD-L1 monotherapy and the combination. We showed that each arm of LY3434172 retained robust binding affinity for its target antigen and that LY3434172 fully blocks PD-1 binding to both PD-L1 and PD-L2 inhibitory ligands, as well as PD-L1 binding to CD80, the ligand for the CD28 costimulatory receptor. LY3434172 resulted in enhanced T-cell activation at lower concentrations relative to each parental antibody and their combination *in vitro*, and enabled bridging of PD-1– and PD-L1–expressing cells. LY3434172 showed slightly reduced activity at higher concentrations compared with the parental antibodies or their combination, which may have resulted from less dual targeting (cell bridging) of the bispecific. LY3434172 therapy resulted in notable and enhanced antitumor activity *in vivo* that was observed in several humanized tumor xenograft models reconstituted with human T cells or PBMCs. In these models, the bispecific antibody demonstrated activity at doses considerably lower than each parental antibody or their combination, and in fact significantly lower than typically observed for biologics in murine models (40). Only the PD-L1 antibody at higher dosage was able to provide similar efficacy as the bispecific. The enhanced potency of LY3434172 was not related to enhanced PK properties of the molecule given the observed normal IgG-like exposure and distribution of the bispecific in mice. The observed superiority of LY3434172 compared with the combination of the parental anti–PD-1 and anti–PD-L1 antibodies suggested that this bispecific had created a unique biological effect. These effects could have been related to the bridging of cells by the bispecific antibody as evidenced by increased PD-1 and PD-L1 interactions over the baseline levels across assay systems or through enhanced development of the immune synapses.

Although not fully understood, the blocking of CD80 binding to PD-L1 on APCs enables CD80 to interact with CTLA-4 resulting in immune suppression and T-cell costimulation through CD28 (15, 16). Further exploration in relevant primary cell models is needed to understand how PD-1 pathway blockade by LY3434172 may influence CD28 and CTLA-4 pathways. In addition, the interplay between innate and adaptive immune cells that express PD-1 pathway targets may potentially be impacted by LY3434172 therapy to generate enhanced T-cell activation. NK cells can mediate antitumor response to PD-1 pathway inhibitors (41). PD-1 antibody blockade on myeloid cells, or myeloid-specific PD-1 genetic ablation, induces antitumor immunity through metabolic reprogramming that leads to increased T effector memory cells (42). The tumor phagocytic activity of tumor-associated macrophages is enhanced by PD-1 or PD-L1 blockade resulting in reduced tumor burden (43).

Given the complex nature of PD-1 pathway interactions and multiple functions in regulating immune response, further mechanistic studies of this human bispecific LY3434172 are needed. However, the humanized mouse tumor models do not fully recapitulate the human immune repertoire, with both adaptive and innate immune cells and respective receptor–ligand pathway molecules, in addition to not capturing human tumor heterogeneity. The observed limited efficacy of anti–PD-1 including the combination of anti–PD-1 and anti–PD-L1 in these models reconstituted with human immune cells was suggestive of inherent limitations and the lack of full translatability. These limitations highlight the need to appropriately evaluate the antitumor biological activity of LY3434172 in the clinical setting.

In summary, our findings with LY3434172 demonstrated how pairing anti–PD-1 and anti–PD-L1 as a dual bispecific enhances the potency of T-cell activation *in vitro* and *in vivo* at low concentrations. These results suggested that dual blockade of both PD-1 and PD-L1 targets with LY3434172 may provide synergy and unique pathway modulation not achievable by single agent PD-1 or PD-L1 or combination immune checkpoint therapy. There is a significant need to develop drug modalities that work effectively at lower dosing to potentially improve tumor penetration and efficacy. LY3434172 is currently under evaluation in patients with advanced cancer (clinical trial NCT03936959).

Disclosure of Potential Conflicts of Interest

H. Kotanides reports employment as a senior research advisor with Eli Lilly and Company and ownership of Eli Lilly and Company shares. Y. Li reports a patent for US20190010232 pending. Y. Shen reports a patent for US20190010232 pending. M. Topper reports employment with Eli Lilly and Company and owns Eli Lilly and Company stock. Y. Lao reports employment with Eli Lilly and Company outside the submitted work. J.N. Haidar reports employment as a research advisor with Eli Lilly and Company. R.D. Novosiadly reports ownership of Eli Lilly and Company and Bristol-Myers Squibb stock outside the submitted work. G.D. Plowman reports personal fees from Eli Lilly and Company (employee through January 15, 2020) outside the submitted work, as well as a patent for US20190010232 pending. D.L. Ludwig reports personal fees from Eli Lilly and Company and Actinium Pharmaceuticals outside the submitted work, as well as a patent for US20190010232 pending. M. Kalos reports prior employment with Eli Lilly and Company and ownership of Eli Lilly and Company stock outside the submitted work, as well as a patent for US20190010232 pending. No potential conflicts of interest were disclosed by the other authors.

Authors' Contributions

H. Kotanides: Conceptualization, supervision, writing–original draft, writing–review and editing. **Y. Li:** Conceptualization, supervision. **M. Malabunga:** Formal analysis, methodology. **C. Carpenito:** Conceptualization, supervision. **S.W. Eastman:** Conceptualization, formal analysis, supervision, methodology. **Y. Shen:** Conceptualization, supervision. **G. Wang:** Formal analysis, methodology. **I. Inigo:** Formal analysis, methodology. **D. Surguladze:** Conceptualization, formal analysis, supervision, methodology. **A.L. Pennello:** Formal analysis, methodology. **K. Persaud:** Conceptualization, supervision. **S. Hindi:** Conceptualization, supervision. **M. Topper:** Formal analysis, methodology. **X. Chen:** Formal analysis, methodology. **Y. Zhang:** Formal analysis, methodology. **D.K. Bulaon:** Formal analysis, methodology. **T. Bailey:** Formal analysis, methodology. **Y. Lao:** Conceptualization, supervision. **B. Han:** Conceptualization, formal analysis, supervision. **S. Torgerson:** Formal analysis, methodology. **D. Chin:** Methodology. **A. Sonyi:** Methodology. **J.N. Haidar:** Conceptualization. **R.D. Novosiadly:** Conceptualization, supervision. **C.M. Moxham:** Conceptualization, supervision. **G.D. Plowman:** Conceptualization, supervision, writing–review and editing. **D.L. Ludwig:** Conceptualization, supervision, writing–review and editing. **M. Kalos:** Conceptualization, supervision, writing–original draft, writing–review and editing.

Acknowledgments

The authors thank Nathan Bayes for helpful scientific discussions, Jason R. Manro for statistical analysis, and Carl June (University of Pennsylvania, Philadelphia, PA) for providing the OV79.FFLuc-2A-gfp tumor cell line. This research was supported by Eli Lilly and Company.

The costs of publication of this article were defrayed in part by the payment of page charges. This article must therefore be hereby marked *advertisement* in accordance with 18 U.S.C. Section 1734 solely to indicate this fact.

Received April 17, 2020; revised June 3, 2020; accepted July 24, 2020; published first July 27, 2020.

References

1. Gong J, Chehrazi-Raffle A, Reddi S, Salgia R. Development of PD-1 and PD-L1 inhibitors as a form of cancer immunotherapy: a comprehensive review of registration trials and future considerations. J Immunother Cancer 2018;6:8.
2. Alsaab HO, Sau S, Alzhrani R, Tatiparti K, Bhise K, Kashaw SK, et al. PD-1 and PD-L1 checkpoint signaling inhibition for cancer immunotherapy: mechanism, combinations, and clinical outcome. Front Pharmacol 2017;8:561.
3. Callahan MK, Postow MA, Wolchok JD. Targeting T cell co-receptors for cancer therapy. Immunity 2016;44:1069–78.
4. Topalian SL, Hodi FS, Brahmer JR, Gettinger SN, Smith DC, McDermott DF, et al. Five-year survival and correlates among patients with advanced melanoma, renal cell carcinoma, or non-small cell lung cancer treated with nivolumab. JAMA Oncol 2019;5:1411–20.
5. Zou W, Wolchok JD, Chen L. PD-L1 (B7-H1) and PD-1 pathway blockade for cancer therapy: mechanisms, response biomarkers, and combinations. Sci Transl Med 2016;8:328rv4.
6. Demaria O, Cornen S, Daëron M, Morel Y, Medzhitov R, Vivier E. Harnessing innate immunity in cancer therapy. Nature 2019;574:45–56.
7. Sharpe AH, Pauken KE. The diverse functions of the PD1 inhibitory pathway. Nat Rev Immunol 2018;18:153–67.
8. Patel SP, Kurzrock R. PD-L1 expression as a predictive biomarker in cancer immunotherapy. Mol Cancer Ther 2015;14:847–56.
9. Mazanet MM, Hughes CC. B7-H1 is expressed by human endothelial cells and suppresses T cell cytokine synthesis. J Immunol 2002;169:3581–8.
10. Xiao Y, Yu S, Zhu B, Bedoret D, Bu X, Francisco LM, et al. RGMb is a novel binding partner for PD-L2 and its engagement with PD-L2 promotes respiratory tolerance. J Exp Med 2014;211:943–59.
11. Chemnitz JM, Parry RV, Nichols KE, June CH, Riley JL. SHP-1 and SHP-2 associate with immunoreceptor tyrosine-based switch motif of programmed death 1 upon primary human T cell stimulation, but only receptor ligation prevents T cell activation. J Immunol 2004;173:945–54.
12. Yokosuka T, Takamatsu M, Kobayashi-Imanishi W, Hashimoto-Tane A, Azuma M, Saito T. Programmed cell death 1 forms negative costimulatory microclusters that directly inhibit T cell receptor signaling by recruiting phosphatase SHP2. J Exp Med 2012;209:1201–17.
13. Patsoukis N, Duke-Cohan JS, Chaudhri A, Aksoylar HI, Wang Q, Council A, et al. Interaction of SHP-2 SH2 domains with PD-1 ITSM induces PD-1 dimerization and SHP-2 activation. Commun Biol 2020;3:128.
14. Chaudhri A, Xiao Y, Klee AN, Wang X, Zhu B, Freeman GJ. PD-L1 binds to B7-1 only in cis on the same cell surface. Cancer Immunol Res 2018;6:921–29.
15. Sugiura D, Maruhashi T, Okazaki IM, Shimizu K, Maeda TK, Takemoto T, et al. Restriction of PD-1 function by cis-PD-L1/CD80 interactions is required for optimal T cell responses. Science 2019;364:558–66.
16. Zhao Y, Lee CK, Lin CH, Gassen RB, Xu X, Huang Z, et al. PD-L1:CD80 cis-heterodimer triggers the co-stimulatory receptor CD28 while repressing the inhibitory PD-1 and CTLA-4 pathways. Immunity 2019;51:1059–73.
17. Khunger M, Hernandez AV, Pasupuleti V, Rakshit S, Pennell NA, Stevenson J, et al. Programmed cell death 1 (PD-1) ligand (PD-L1) expression in solid tumors as a predictive biomarker of benefit from PD-1/PD-L1 axis inhibitors: a systematic review and meta-analysis. JCO Precis Oncol 2017;1:1–15.
18. Teng F, Meng X, Kong L, Yu J. Progress and challenges of predictive biomarkers of anti PD-1/PD-L1 immunotherapy: a systematic review. Cancer Lett 2018;414:166–73.
19. Ott PA, Hodi FS, Kaufman HL, Wigginton JM, Wolchok JD. Combination immunotherapy: a road map. J Immunother Cancer 2017;5:16.
20. Larkin J, Chiarion-Sileni V, Gonzalez R, Grob JJ, Rutkowski P, Lao CD, et al. Five-year survival with combined nivolumab and ipilimumab in advanced melanoma. N Engl J Med 2019;381:1535–46.
21. Rotte A. Combination of CTLA-4 and PD-1 blockers for treatment of cancer. J Exp Clin Cancer Res 2019;38:255.
22. Gandhi L, Rodríguez-Abreu D, Gadgeel S, Esteban E, Felip E, De Angelis F, et al. Pembrolizumab plus chemotherapy in metastatic non-small-cell lung cancer. N Engl J Med 2018;378:2078–92.
23. Borghaei H, Langer CJ, Gadgeel S, Papadimitrakopoulou VA, Patnaik A, Powell SF, et al. 24-month overall survival from KEYNOTE-021 cohort G: pemetrexed and carboplatin with or without pembrolizumab as first-line therapy for advanced nonsquamous non-small cell lung cancer. J Thorac Oncol 2019;14:124–29.
24. Socinski MA, Jotte RM, Cappuzzo F, Orlandi F, Stroyakovskiy D, Nogami N, et al. Atezolizumab for first-line treatment of metastatic nonsquamous NSCLC. N Engl J Med 2018;378:2288–301.
25. Brahmer JR, Drake CG, Wollner I, Powderly JD, Picus J, Sharfman WH, et al. Phase I study of single-agent anti-programmed death-1 (MDX-1106) in refractory solid tumors: safety, clinical activity, pharmacodynamics, and immunologic correlates. J Clin Oncol 2010;28:3167–75.
26. Agrawal S, Feng Y, Roy A, Kollia G, Lestini B. Nivolumab dose selection: challenges, opportunities, and lessons learned for cancer immunotherapy. J Immunother Cancer 2016;4:72.
27. Das R, Verma R, Sznol M, Boddupalli CS, Gettinger SN, Kluger H, et al. Combination therapy with anti-CTLA-4 and anti-PD-1 leads to distinct immunologic changes in vivo. J Immunol 2015;194:950–9.
28. Burrack AL, Spartz EJ, Raynor JF, Wang I, Olson M, Stromnes IM. Combination PD-1 and PD-L1 blockade promotes durable neoantigen-specific T cell-mediated immunity in pancreatic ductal adenocarcinoma. Cell Rep 2019;28:2140–55.
29. Hamid O, Chow LQ, Sanborn RE, Marshall S, Black C, Gribbin M, et al. Combination of MEDI0680, an anti-PD-1 antibody, with durvalumab, an anti-PD-L1 antibody: a phase 1, open-label study in advanced malignancies. Ann Oncol 2016;27:vi359–78.
30. Spiess C, Zhai Q, Carter PJ. Alternative molecular formats and therapeutic applications for bispecific antibodies. Mol Immunol 2015;67:95–106.
31. Dahlén E, Veitonmäki N, Norlén P. Bispecific antibodies in cancer immunotherapy. Ther Adv Vaccines Immunother 2018;6:3–17.
32. Labrijn AF, Janmaat ML, Reichert JM, Parren PWHI. Bispecific antibodies: a mechanistic review of the pipeline. Nat Rev Drug Discov 2019;18:585–608.
33. Strauss J, Heery CR, Schlom J, Madan RA, Cao L, Kang Z, et al. Phase I trial of M7824 (MSB0011359C), a bifunctional fusion protein targeting PD-L1 and TGFβ, in advanced solid tumors. Clin Cancer Res 2018;24:1287–95.
34. Von Kreudenstein TS, Escobar-Carbrera E, Lario PI, D'Angelo I, Brault K, Kelly J, et al. Improving biophysical properties of a bispecific antibody scaffold to aid developability: quality by molecular design. MAbs 2013;5:646–54.
35. Zhang S, Zhang M, Wu W, Yuan Z, Tsun A, Wu M, et al. Preclinical characterization of sintilimab, a fully human anti-PD-1 therapeutic monoclonal antibody for cancer. Antibody Ther 2018;1:65–73.
36. Li Y, Carpenito C, Wang G, Surguladze D, Forest A, Malabunga M, et al. Discovery and preclinical characterization of the antagonist anti-PD-L1 monoclonal antibody LY3300054. J Immunother Cancer 2018;6:31.
37. Bertozzi CC, Chang CY, Jairaj S, Shan X, Huang J, Weber BL, et al. Multiple initial culture conditions enhance the establishment of cell lines from primary ovarian cancer specimens. In Vitro Cell Dev Biol Anim 2006;42:58–62.
38. Brown JA, Dorfman DM, Ma FR, Sullivan EL, Munoz O, Wood CR, et al. Blockade of programmed death-1 ligands on dendritic cells enhances T cell activation and cytokine production. J Immunol 2003;170:1257–66.
39. Zhao Y, Harrison DL, Song Y, Jie J, Huang J, Hui E. Antigen-presenting cell-intrinsic PD-1 neutralizes PD-L1 in cis to attenuate PD-1 signaling in T cells. Cell Rep 2018;24:379–90.
40. Lin S, Huang G, Cheng L, Li Z, Xiao Y, Deng Q, et al. Establishment of peripheral blood mononuclear cell-derived humanized lung cancer mouse models for studying efficacy of PD-L1/PD-1 targeted immunotherapy. MAbs 2018;10:1301–11.
41. Hsu J, Hodgins JJ, Marathe M, Nicolai CJ, Bourgeois-Daigneault MC, Trevino TN, et al. Contribution of NK cells to immunotherapy mediated by PD-1/PD-L1 blockade. J Clin Invest 2018;128:4654–68.
42. Strauss L, Mahmoud MAA, Weaver JD, Tijaro-Ovalle NM, Christofides A, Wang Q, et al. Targeted deletion of PD-1 in myeloid cells induces antitumor immunity. Sci Immunol 2020;5:eaay1863.
43. Gordon SR, Maute RL, Dulken BW, Hutter G, George BM, McCracken MN, et al. PD-1 expression by tumour-associated macrophages inhibits phagocytosis and tumour immunity. Nature 2017;545:495–99.